

UNCLASSIFIED

AD 274 648

*Reproduced
by the*

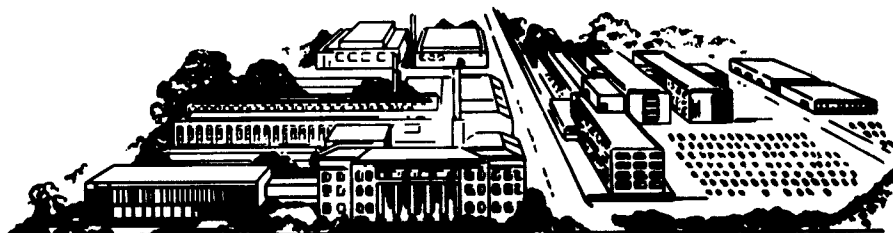
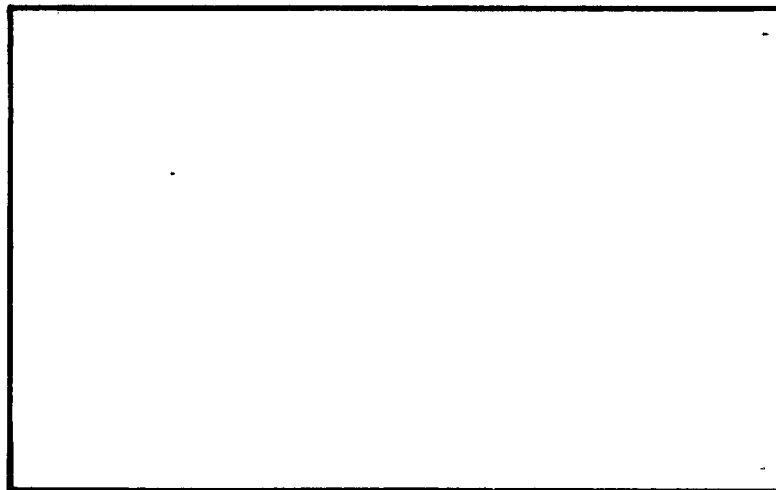
**ARMED SERVICES TECHNICAL INFORMATION AGENCY
ARLINGTON HALL STATION
ARLINGTON 12, VIRGINIA**



UNCLASSIFIED

NOTICE: When government or other drawings, specifications or other data are used for any purpose other than in connection with a definitely related government procurement operation, the U. S. Government thereby incurs no responsibility, nor any obligation whatsoever; and the fact that the Government may have formulated, furnished, or in any way supplied the said drawings, specifications, or other data is not to be regarded by implication or otherwise as in any manner licensing the holder or any other person or corporation, or conveying any rights or permission to manufacture, use or sell any patented invention that may in any way be related thereto.

274648

CATALOGED BY ASTIA
AS AD NO.**RESEARCH REPORT****BATTELLE**
MEMORIAL INSTITUTEASTIA
RECEIVED
APR 30 1962
JISIA
B

TOPICAL REPORT

on

**HEAT TRANSFER TO A SOLID-
PROPELLANT ROCKET-MOTOR NOZZLE**

to

**AERONAUTICAL SYSTEMS DIVISION
WRIGHT-PATTERSON AIR FORCE BASE**

December 30, 1961

by

E. W. Ungar

**Contract No. AF 33(616)-6358
Task No. 73500**

**BATTELLE MEMORIAL INSTITUTE
505 King Avenue
Columbus 1, Ohio**

FOREWORD

This topical report was prepared by Battelle Memorial Institute for the United States Air Force on Contract No. AF 33(616)-6358. The contract was initiated under Project No. 7350 and Task No. 73500. The work is administered under the direction of the Ceramics and Graphite Branch, Metals and Ceramics Laboratory, Directorate of Materials and Processes, Aeronautical Systems Division, with Lt. T. E. Lippart acting as Project Engineer. This report covers work conducted from September, 1960, through June, 1961.

DISTRIBUTION LIST

National Aeronautics & Space
Administration (7)
1520 H Street, N. W.
Washington 25, D. C.
Attn: Chief, Division of Research
Information

Headquarters (1)
6593rd Test Group (Dev)
Air Force Systems Command
United States Air Force
Edwards Air Force Base, California
Attn: (DGS)

Headquarters, Space Systems
Division (1)
Air Force Systems Command
P. O. Box 262
Air Force Unit Post Office
Los Angeles 45, California
Attn: TDC

Commander (10)
Armed Services Tech. Information
Agency
Arlington Hall Station
Arlington 12, Virginia
Attn: TIPCR

Commanding General (1)
Aberdeen Proving Ground
Maryland
Attn: Ballistic Research
Laboratories
ORDBG-BLI

Commanding General (1)
USA Ordnance Arsenal, Frankford
Philadelphia 37, Pennsylvania
Attn: Propellant and Explosives
Section, 1331

Department of the Army (1)
Office, Chief of Ordnance
Washington 25, D. C.
Attn: ORDTB

Commander (4)
Army Rocket and Guided Missile
Agency
Redstone Arsenal
Alabama
Attn: Technical Library
ORDXR-OTL

Commander (1)
Army Ballistic Missile Agency
Redstone Arsenal, Alabama
Attn: ORDAB-HSI

Bureau of Naval Weapons (2)
Department of the Navy
Washington 25, D. C.
Attn: DLI-3

Bureau of Naval Weapons (2)
Department of the Navy
Washington 25, D. C.
Attn: RMMP-2

Bureau of Naval Weapons (1)
Department of the Navy
Washington 25, D. C.
Attn: RMMP-331

Commander (1)
U. S. Naval Air Test Center
Point Mugu, California
Attn: Technical Library

Commanding Officer (1)
U. S. Naval Propellant Plant
Indian Head, Maryland
Attn: Technical Library

Commander (1)
U. S. Naval Ordnance Laboratory
White Oak
Silver Spring, Maryland
Attn: Library

BATTELLE MEMORIAL INSTITUTE

DISTRIBUTION LIST
(Continued)

Commanding Officer (1)
Picatinny Arsenal
Dover, New Jersey
Attn: Library

Director (1)
Special Projects Office
Department of the Navy
Washington 25, D. C.

Aerojet-General Corporation (1)
P. O. Box 296
Azusa, California
Attn: Librarian

Armour Research Foundation (1)
of Illinois Institute of Technology
Technology Center
Chicago 16, Illinois
Attn: Fluid Dynamics & System
Research
Department D

Jet Propulsion Laboratory (1)
4800 Oak Grove Drive
Pasadena 3, California
Attn: I. E. Newlan
Chief, Reports Group

Lockheed Propulsion Company (3)
P. O. Box 111
Redlands, California
Attn: Miss Belle Berlad, Librarian

Aerojet-General Corporation (3)
Box 1947
Sacramento, California
Attn: Technical Information Center

Thiokol Chemical Corporation (1)
Elkton Division
Elkton, Maryland
Attn: Librarian

Commander (1)
U. S. Naval Ordnance Test Station
China Lake, California
Attn: Technical Library Branch

Rocketdyne, A Division of North
American Aviation, Inc. (1)
Solid Propulsion Operations
P. O. Box 548
McGregor, Texas
Attn: Library

American Machine and
Foundry Co. (1)
Mechanics Research Department
7501 North Natchez Avenue
Niles 48, Illinois
Attn: Phil Rosenberg

Rocketdyne (3)
6633 Canoga Avenue
Canoga Park, California
Attn: Library, Department 596-306

Solid Propellant Information
Agency (3)
Applied Physics Laboratory
The Johns Hopkins University
Silver Spring, Maryland

Thiokol Chemical Corporation (2)
Redstone Division
Huntsville, Alabama
Attn: Technical Director

Thiokol Chemical Corporation (2)
Wasatch Division
P. O. Box 524
Brigham City, Utah
Attn: Library Section

DISTRIBUTION LIST
(Continued)

Olin Mathieson Chemical
Corporation (1)
Marion, Illinois
Attn: Research Library
Box 508

Hercules Powder Company (1)
Bacchus Works
Magna, Utah
Attn: Librarian

United Technology Corporation (1)
P. O. Box 358
Sunnyvale, California
Attn: Librarian

Air Force Plant Representative (1)
Thompson Ramo Wooldridge, Inc.
23555 Euclid Avenue
Cleveland 17, Ohio
Attn: Mr. R. H. Hiltz

National Aeronautics and Space
Administration (2)
Lewis Research Center
21000 Brookpark Road
Cleveland 35, Ohio
Attn: George Mandel, Chief,
Library

Thiokol Chemical Corporation (1)
Reaction Motors Division
Denville, New Jersey
Attn: Julius Stock
Materials Engineer

Air Force Plant Representative (1)
General Motors Corporation
Research Laboratories
Metallurgical Engineering Dept.
12 Mile and Mound Roads
Warren, Michigan
Attn: Mr. H. H. Rice

Olin Mathieson Chemical
Corporation (3)
Research Library 1-K-3
275 Winchester Avenue
New Haven, Connecticut
Attn: Mail Control Room
Mrs. Laura M. Kajuti

Ingersoll Kalamazoo Division (1)
Borg-Warner Corporation
1810 N. Pitcher Street
Kalamazoo, Michigan
Attn: J. W. Schiffel
Chief Engineer
Special Projects Department

The B. F. Goodrich Company (1)
Research Center
Brecksville, Ohio
Attn: Charles H. Stockman

Space Technology Laboratories,
Inc. (1)
5730 Arbor-Vitae Street
Los Angeles 45, California
Attn: R. C. Anderson

Commander (1)
AFFTC
Edwards AFB, California
Attn: FTRLC

Hercules Powder Company (1)
Allegany Ballistics Laboratory
P. O. Box 210
Cumberland, Maryland
Attn: Library

National Carbon Company (1)
P. O. Box 6116
Cleveland 1, Ohio
Attn: AML Librarian

DISTRIBUTION LIST
(Continued)

Institute for Defense Analyses (1)
Research and Engineering Support Division
1825 Connecticut Avenue, N. W.
Washington 9, D. C.
Attn: Technical Information Office

TABLE OF CONTENTS

	<u>Page</u>
INTRODUCTION	1
SUMMARY	3
RESEARCH APPROACH	3
Calorimeter Nozzle	4
Numerical Procedures	6
TEST-FIRING RESULTS	12
TEMPERATURE-HISTORY CALCULATIONS	18
CONCLUSIONS	22
REFERENCES	26

APPENDIX

PRESSURE DEPENDENCE ON ALUMINA THICKNESS	A-1
--	-----

LIST OF FIGURES

Figure 1. Schematic of Physical Nature of the Heat-Transfer Problem	2
Figure 2. Molybdenum Calorimeter Nozzle and Thermocouple Arrangement	5
Figure 3. Typical Surface Ring	7
Figure 4. Typical Temperature Histories For Propellant A	14
Figure 5. Typical Temperature Histories For Propellant B	15
Figure 6. Chamber-Pressure Trace For Propellant A Motor.	16
Figure 7. Eigenvalue Variation With N_a	20
Figure 8. Calculated and Experimental Surface Temperatures of Nozzle Inserts Fired in Motors Containing Propellant A	23

LIST OF FIGURES
(Continued)

	<u>Page</u>
Figure 9. Calculated and Experimental Surface Temperatures of Nozzle Inserts Fired in Motors Containing Propellant B	24 24
Figure A-1. Variation of Alumina-Layer Thickness as a Function of Measured Chamber Pressure	A-3 A-3

LIST OF TABLES

Table 1. Heat-Transfer Coefficients	17
Table 2. Mean Property Values For Various Ceramics	21

DEFINITION OF SYMBOLS

A - surface area
a - instantaneous rate of change of T_A
b - instantaneous rate of change of T_S
C - constant of integration
 c_p - specific heat
 F_1 - function defined by Equation (15)
 F_2 - function defined by Equation (16)
h - heat transfer coefficient defined by Equation (24)
k - thermal conductivity
Nu - Nusselt number for the gas-side heat transfer
Pr - Prandtl number for the exhaust products
 \dot{q} - heat flux
 \dot{q}_g - heat flux from the gas to the exposed alumina surface
 \dot{q}_n - heat flux from the alumina to the nozzle
r - radial distance
Re - Reynolds number of the exhaust products
T - temperature
 T_A - temperature at the exposed alumina surface
 T_g - gas temperature
 T_s - temperature at the nozzle surface
t - time
 u_g - gas velocity
 u_l - liquid velocity
V - volume of ring
(Δx) - distance between centers of i rings
(Δr) - distance between centers of i and j rings
 α - thermal diffusivity
 δ - deposit layer thickness
 ρ - density
 $\theta = T - T_{s0}$

Subscripts

i - ith ring
j - jth ring
n - nozzle
0 - initial time ($t = 0$)

HEAT TRANSFER TO A SOLID-PROPELLANT ROCKET-MOTOR NOZZLE*

by

E. W. Ungar

INTRODUCTION

The performance of a nozzle structure during a solid-propellant rocket-motor firing is intimately related to the heat transfer from the hot exhaust products to the nozzle surface. Modern high-energy solid propellants contain large quantities of metal additives. Thus, metal oxides are present in the exhaust, which influence heat-transfer processes.

Figure 1 shows schematically the physical nature of the nozzle heat-transfer problem. There is an oxide layer of thickness δ on the nozzle surface. In general, heat is transferred at a rate \dot{q}_g to the molten oxide layer. In addition, oxide deposits from the gas stream and also flows along the surface. If the nozzle surface temperature is lower than the oxide melting point, there is a liquid-solid interface within the oxide layer. Heat is transferred at a rate \dot{q}_n from the oxide to the nozzle surface. In general, the problem is transient, so $\dot{q}_g \neq \dot{q}_n$, and δ is not a constant.

Early in a rocket-motor firing while the nozzle walls are cool, oxide accumulates on the walls. This oxide is cooled rapidly by conduction to the cold structure. After a short while, the oxide layer grows to an appreciable thickness, thus providing some resistance to heat flow. When the resistance to heat flow becomes sufficiently large, it is possible that the nozzle surface loses heat to the bulk of the nozzle structure faster than it receives heat from the oxide, resulting in a temporary drop in surface temperature. The hot exhaust products then begin to reheat the oxide. As heating continues, the layer thickness begins to decrease. If the nozzle surface temperature reaches the oxide's melting point, all of the oxide on the surface is molten.

In order to define the exposure conditions of a nozzle material, it would be desirable to define either the nozzle surface temperature, T_s , and/or the heat flux, \dot{q}_n , as functions of time. These quantities are, of course, dependent on \dot{q}_g , δ , and the physical properties of the oxide. To provide a

* A supplementary study made in conjunction with Air Force Contract No. AF 33(616)-6358 which concerned an investigation of nozzle-failure mechanisms in solid-propellant rockets for the Aeronautical Systems Division, Wright-Patterson Air Force Base, Ohio.

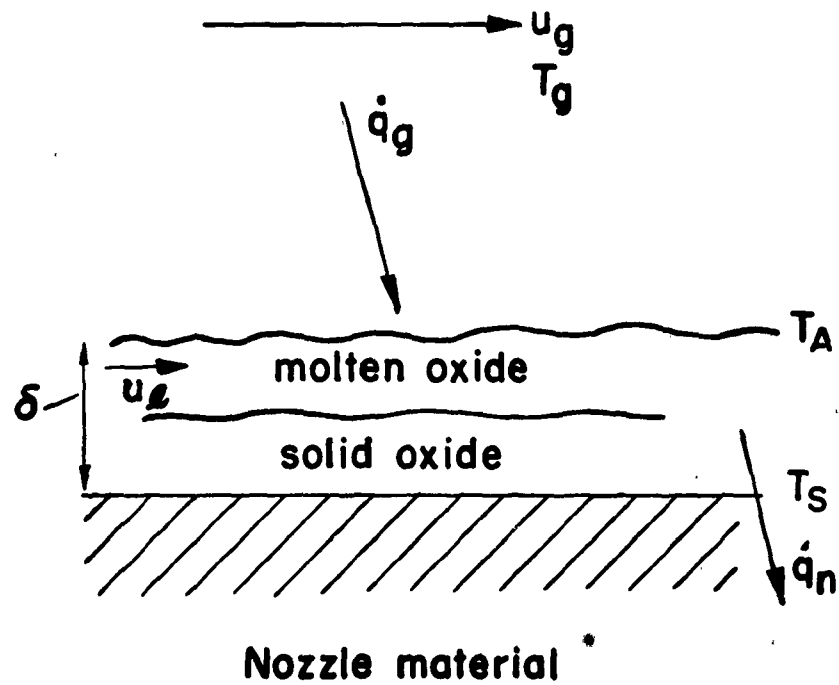


FIGURE 1. SCHEMATIC OF PHYSICAL NATURE OF THE HEAT-TRANSFER PROBLEM

basis for extrapolating \dot{q}_w to other than the particular set of test conditions, it is desirable to relate it to a heat-transfer coefficient and the temperature difference between the gas and the outer edge of the oxide layer.

SUMMARY

The heat transfer to a small-scale rocket nozzle was studied under the conditions imposed by the combustion of two high-energy solid propellants. The exhaust ~~products of these propellants~~ contain large quantities of aluminum oxide. The heat-transfer problem can be separated into (1) the heat transfer from the hot combustion products to a layer of deposited alumina and (2) the heat transfer from the alumina layer to the underlying solid material. ~~The~~ temperature histories at several locations in ~~molybdenum~~ ^{MIB} nozzles were measured with high-temperature thermocouples. ~~Surface temperatures in excess of the melting point of alumina could be measured with these thermocouples. The measured temperatures were used to~~ numerically compute the heat-transfer rate from the deposited alumina to the nozzles. ~~Analysis showed that during some periods of the motor firings, the heat transfer across the alumina layer could be deduced from steady-state relations. The thickness of the alumina layer was estimated at the throat on the basis of the measured chamber pressure and propellant burning rate characteristics. Using this estimated thickness, the temperature at the exposed alumina surface and the heat-transfer coefficient between the combustion products and the alumina could be determined. The and heat-transfer coefficients which were determined in this manner agreed with those determined from ordinary turbulent heat-transfer theory. This agreement indicates that, although the alumina-deposit layer insulates the nozzle structure (and in so doing strongly influences the temperature history), the effect of the depositing alumina droplets on gas-side convective heat transfer is negligible. The heat-transfer coefficients determined in this study were applied to the computation of nozzle surface-temperature history for various ceramic nozzle materials. Calculations successfully predicted the time in the firing at which melting or thermal degradation occurred.~~

RESEARCH APPROACH

Studies were carried out using small-scale solid-propellant rocket motors. Motor and nozzle configurations had been previously chosen for materials evaluations. Two high-energy propellants were employed in the program. These were: (1) a composite propellant containing 16 per cent aluminum (Propellant A) and (2) a double-base propellant containing 21 per cent aluminum (Propellant B).

The over-all procedure was to measure temperatures at various positions in a test nozzle during motor firings. The temperature histories were used to compute the heat-transfer rate into the nozzle surface, \dot{q}_n . Chamber-pressure data were used to determine the aluminum oxide layer thickness at the throat, δ . Aluminum oxide property data were then used in conjunction with a procedure described below to compute the exposed alumina surface temperature and heat flux, \dot{q}_g . A heat-transfer coefficient between the gas and the alumina layer was then computed and compared with values computed by ordinary methods. An inverse procedure was then used to determine the temperature history of several nozzle materials.

Calorimeter Nozzle

The short-time transients involved in a solid-propellant rocket-motor firing required that the measurement scheme be capable of quick response. Surface temperature responds rapidly to environmental changes and so was used to determine heat-transfer rates. Convergent test nozzles were fabricated from molybdenum because its thermal properties are reasonably well known, and because it is machinable, available, and suitable for operation above 4000 F.

Figure 2 shows the test nozzle and thermocouple arrangement. The nozzles were instrumented with ten tungsten-rhenium thermocouples. Each thermocouple wire had a diameter of 0.010 inch and was coated with 0.002 inch of magnesia to provide insulation when placed in the 0.016-inch holes in the nozzle. Junctions for five of the thermocouples were located 0.0125 inch from the exposed surface of the nozzle, and junctions for the remaining five were 0.0875 inch from the surface. Each wire was resistance welded to the bottom of a hole, two holes being used for each couple. The thermocouple wires were dispersed around the circumference of the nozzle into 16 positions, each couple being separated by 90 degrees. Thermocouple outputs were recorded on a high-speed CEC galvanometer recorder. The combined response of the thermocouple and recorder is believed to be better than 1 millisecond.

The placement of each thermocouple wire in a separate hole was required because of the necessity of minimizing temperature-distribution disturbances caused by the presence of the thermocouples. Because of the physical arrangement of the nozzle on the rocket motor, it was not possible to drill the thermocouple holes along isotherms. The disturbance caused by the presence of thermocouples was assumed to be small because of the small size of the holes and the fact that both tungsten and rhenium are better thermal conductors than molybdenum.

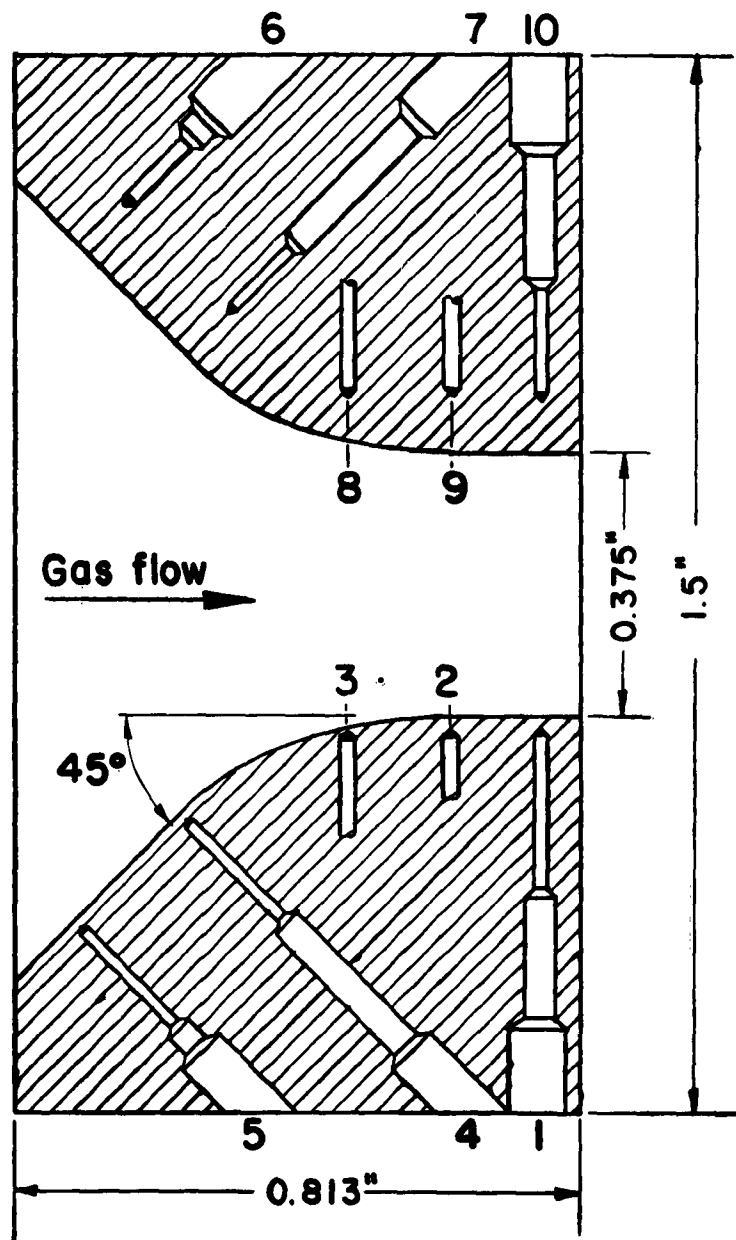


FIGURE 2. MOLYBDENUM CALORIMETER NOZZLE AND THERMOCOUPLE ARRANGEMENT

With the two-hole arrangement, each thermocouple consisted of a tungsten-molybdenum and a molybdenum-rhenium junction. The molybdenum cancels so long as the two junctions are close in temperature. The two junctions, although at different angular positions, were at the same depth and axial positions. Measured temperatures are, therefore, an average of two temperatures measured at different angular positions. Thermocouples arranged in this manner were calibrated in an induction furnace up to 2000 F. The observed millivolt output was that expected from an ordinary tungsten-rhenium thermocouple.

Numerical Procedures

The determination of the heat flux at the nozzle surface, \dot{q}_n , was based on a network approximation developed for this study. In order to provide meaningful results, the procedure had to account for both the variation in molybdenum properties with temperature and axial conduction of heat along the nozzle.

The nozzle was considered as a series of rings. A heat balance was carried out for each ring. The general procedure was similar to those described by Jakob^{(1)*} and Dusenberre⁽²⁾ with the exception that the expressions for the interface area between rings was complicated by the nozzle shape.

Figure 3 shows a typical ring. A heat balance for the i^{th} surface ring can be written as

$$\begin{aligned} \dot{q}_{n,i} A_i \Delta t + A_{i-1,i} k \frac{(T_{i-1} - T_i)}{(\Delta x)_{i-1,i}} \Delta t \\ + A_{i,i+1} k \frac{(T_{i+1} - T_i)}{(\Delta x)_{i,i+1}} \Delta t + A_{i,j} k \frac{(T_j - T_i)}{(\Delta r)_{i,j}} \Delta t \\ = \rho_n c_{pn} V_i (T_{i,\Delta t} - T_i) , \end{aligned} \quad (1)$$

where the areas and volumes are obtained from geometric considerations.

The thermocouples were placed at the center of rings so that the T_i 's and T_j 's could be obtained from experiment. Only the heat flux at the surface was sought, so the only rings of interest were the surface rings and the rings in the layer immediately behind them. The interface between the i and j rings was chosen so as to be approximately parallel with the expected isotherms. An IBM 650 computer was used for the calculation of the local heat flux, \dot{q}_{ni} , from the measured temperatures.

* Numbers in parentheses refer to references listed at the end of this report.

\mathcal{Q}

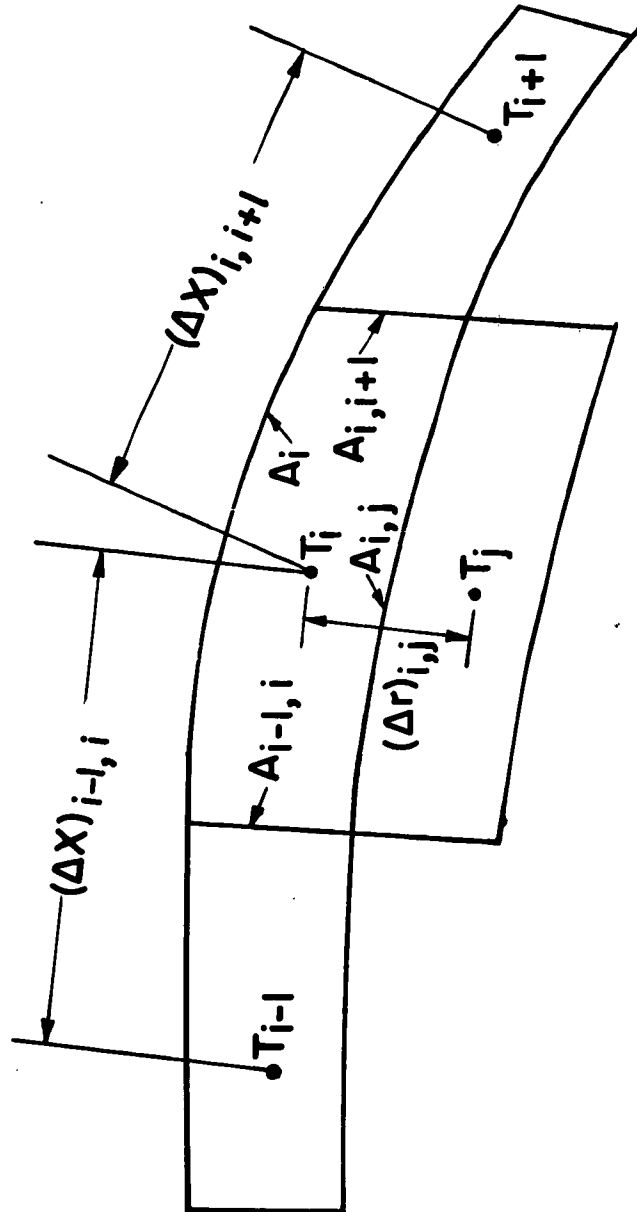


FIGURE 3. TYPICAL SURFACE RING

The program allowed variable thermal properties to be included in the calculation. The thermal properties presented by Rasor and McClelland⁽³⁾ were used in the computation. There is some disagreement between the thermal-conductivity data in Reference (3) and those presented in the compilation by Goldsmith and Waterman⁽⁴⁾. Due to the grade of the molybdenum used in this program, the data from Reference 3 were preferred.

The computer program described above provides the local heat flux at the nozzle surface. The aluminum oxide layer on the surface must be analyzed to determine the gas-side heat flux, q_g , and the temperature at the exposed alumina surface, T_A . The layer is thin and can be approximated by a slab with an arbitrary time variation in temperature imposed at both faces. If, in the temperature range of interest, the thermal conductivity and diffusivity are assumed to be constant, then the heat-conduction equation becomes

$$\frac{\partial^2 \theta}{\partial r^2} = \frac{1}{\alpha} \frac{\partial \theta}{\partial t}, \quad (2)$$

with the boundary conditions

$$r = 0, \theta = \theta_A(t) \quad (3)$$

$$r = \delta, \theta = \theta_S(t)$$

$$t = 0, \theta = \theta_O(r),$$

where $\theta = T - T_{S0}$, and $r = 0$ is chosen to be the gas-side face of the alumina layer.

The presence of a possible solid-liquid interface within the deposit layer was neglected because of the low latent heat of fusion of alumina and low liquid-film-flow velocities. The layer thickness, δ , was assumed to be constant for the analysis.

Following Carslaw and Jaeger⁽⁵⁾, let

$$\theta = \theta_1 + \theta_2, \quad (4)$$

with

$$\frac{\partial^2 \theta_1}{\partial r^2} = \frac{1}{\alpha} \frac{\partial \theta_1}{\partial t}, \quad (5)$$

and at

$$r = 0, \theta_1 = 0 \quad (6)$$

$$r = \delta, \theta_1 = 0$$

$$t = 0, \theta_1 = \theta_O(r).$$

Also,

$$\frac{\partial^2 \theta_2}{\partial r^2} = \frac{1}{\alpha} \frac{\partial \theta_2}{\partial t}, \quad (7)$$

and at

$$r = 0, \theta_2 = \theta_A(t) \quad (8)$$

$$r = \delta, \theta_2 = \theta_s(t)$$

$$t = 0, \theta_2 = 0.$$

Equation (5) has a solution

$$\theta_1 = e^{-\alpha \lambda^2 t} (C_1 \cos \lambda r + C_2 \sin \lambda r). \quad (9)$$

Introduction of the boundary conditions on r from Equation (6) leads to

$$\theta_1 = \sum_{n=1}^{\infty} C_n e^{-\alpha n^2 \pi^2 t / \delta^2} \sin \frac{n\pi r}{\delta}. \quad (10)$$

At time $t = 0$,

$$\theta_1 = \theta_0(r) = \sum_{n=1}^{\infty} C_n \sin \frac{n\pi r}{\delta}, \quad (11)$$

which is simply a Fourier series for the function $\theta_0(r)$ with constant coefficients C_n given by

$$C_n = \frac{2}{\delta} \int_0^{\delta} \theta_0(r) \sin \frac{n\pi r}{\delta} dr. \quad (12)$$

Thus,

$$\theta_1 = \frac{2}{\delta} \sum_{n=1}^{\infty} e^{-\alpha n^2 \pi^2 t / \delta^2} \sin \frac{n\pi r}{\delta} \int_0^{\delta} \theta_0 \sin \frac{n\pi r}{\delta} dr. \quad (13)$$

Duhamel's Theorem⁽⁵⁾ is relied on for the solution to Equation (7).

Thus,

$$\theta_2 = \int_0^t \left[\theta_A(\tau) \frac{\partial F_1}{\partial t}(r, t-\tau) + \theta_s \frac{\partial F_2}{\partial t}(r, t-\tau) \right] d\tau. \quad (14)$$

Integration by parts yields

$$\begin{aligned} \theta_2 = & \theta_A(0) F_1(r, t) + \theta_s(0) F_2(r, t) \\ & + \int_0^t [\dot{\theta}_A(\tau) F_1(r, t - \tau) + \dot{\theta}_s(\tau) F_2(r, t - \tau)] d\tau, \end{aligned} \quad (15)$$

where the dot denotes differentiation with respect to time. The function $F(r, t)$ represents the temperature at the time t in which the initial temperature is zero and F_1 is unity at $r = 0$ and zero at $r = \delta$, F_2 is unity at $r = \delta$ and zero at $r = 0$. Thus,

$$F_1(r, t - \tau) = 1 - \frac{r}{\delta} - \frac{2}{\pi} \sum_{n=1}^{\infty} \frac{1}{n} e^{-\alpha n^2 \pi^2 (t - \tau) / \delta^2} \sin \frac{n\pi r}{\delta}, \quad (16)$$

$$F_2(r, t - \tau) = \frac{r}{\delta} + \frac{2}{\pi} \sum_{n=1}^{\infty} \frac{\cos n\pi}{n} e^{-\alpha n^2 \pi^2 (t - \tau) / \delta^2} \sin \frac{n\pi r}{\delta}.$$

Combining Equations (15) and (16), leads to

$$\begin{aligned} \theta_2 = & \left(1 - \frac{r}{\delta}\right) \theta_A + \frac{r}{\delta} \theta_s + \frac{2}{\pi} \sum_{n=1}^{\infty} \frac{1}{n} e^{-\alpha n^2 \pi^2 t / \delta^2} \sin \frac{n\pi r}{\delta} \\ & \times \left\{ \left[(-1)^n \theta_s(0) - \theta_A(0) \right] + \int_0^t e^{+\alpha n^2 \pi^2 \tau / \delta^2} \left[(-1)^n \dot{\theta}_s - \dot{\theta}_A \right] d\tau \right\}. \end{aligned} \quad (17)$$

Finally,

$$\begin{aligned} \theta = & \left(1 - \frac{r}{\delta}\right) \theta_A + \frac{r}{\delta} \theta_s + \frac{2}{\delta} \sum_{n=1}^{\infty} e^{-\alpha n^2 \pi^2 t / \delta^2} \sin \frac{n\pi r}{\delta} \int_0^{\delta} \theta_0 \sin \frac{n\pi r}{\delta} dr \\ & - \frac{2}{\pi} \sum_{n=1}^{\infty} \frac{1}{n} e^{-\alpha n^2 \pi^2 t / \delta^2} \sin \frac{n\pi r}{\delta} \left\{ \left[\theta_A(0) - (-1)^n \theta_s(0) \right] \right. \\ & \left. + \int_0^t e^{+\alpha n^2 \pi^2 \tau / \delta^2} \left[\dot{\theta}_A - (-1)^n \dot{\theta}_s \right] d\tau \right\}. \end{aligned} \quad (18)$$

Equation (18) is not identical to the form obtained in Reference (5) but is considered more suited to this particular problem. The difference arises because of a difference in the manner in which Duhamel's Theorem was integrated (both forms are equivalent). The resulting Equation (18) is actually the limit of the expression obtained in Reference (5).

Evaluation of the time integral in Equation (18) showed that the products of its value and the value of the negative exponential in time are not affected by $\dot{\theta}_A$ or $\dot{\theta}_S$ prior to 0.01 second of the point in time under consideration for the thickness encountered and the properties of alumina. The exponential becomes quite small after short times for the thin alumina layer so that the initial time contributions in Equation (18) are negligible.

Equation (18) can be differentiated with respect to r to yield the heat flux. Neglecting the initial time contributions

$$\dot{q} = -k \frac{\partial \theta}{\partial r} = \frac{k}{\delta} (\theta_A - \theta_S) + \frac{2k}{\delta} \sum_{n=1}^{\infty} e^{-\alpha n^2 \pi^2 t / \delta^2} \cos \frac{n\pi r}{\delta} \times \int_0^t e^{\alpha n^2 \pi^2 \tau / \delta^2} \left[\dot{\theta}_A - (-1)^n \dot{\theta}_S \right] d\tau. \quad (19)$$

Evaluation of Equation (19) at $r = 0$ and $r = \delta$, and combination lead to

$$\dot{q}_g = \dot{q}_n + \frac{2k}{\delta} \sum_{n=1}^{\infty} [1 - (-1)^n] e^{-\alpha n^2 \pi^2 t / \delta^2} \int_0^t [\dot{\theta}_A + \dot{\theta}_S] e^{\alpha n^2 \pi^2 \tau / \delta^2} d\tau. \quad (20)$$

For the case of the alumina layer on the nozzle surface, evaluation of the series shows that Equation (20) is closely approximated by

$$\dot{q}_g = \dot{q}_n + \frac{1}{2} (a + b) \rho c_p \delta, \quad (21)$$

where a and b are the instantaneous rates of change of T_A and T_S .

The experimental data showed that

$$\dot{q}_n \gg \frac{1}{2} (a + b) \rho c_p \delta,$$

so that for the conditions in a solid-propellant rocket-motor nozzle the alumina layer could be analyzed on the basis of a steady-state heat-transfer equation with a small correction of $\frac{1}{2} (a + b) \rho c_p \delta$. The temperature at the exposed alumina surface, T_A , could be found from

$$\dot{q}_g \approx \dot{q}_n \approx \frac{k}{\delta} (T_A - T_s), \quad (22)$$

or

$$T_A = T_s + \frac{\dot{q}_n \delta}{k}. \quad (23)$$

These equations are considered to be valid during any time period of the motor firing that the alumina layer thickness, δ , is approximately constant.

Based on a temperature difference, the heat-transfer coefficient is

$$h = \frac{\dot{q}_g}{T_g - T_A}. \quad (24)$$

The calculation procedure was iterative. The value of \dot{q}_n was obtained from the measured temperatures by means of the program described earlier. The temperature T_A was obtained from Equation (23). The alumina thermal-conductivity values used in Equation (23) were those presented by McQuarrie(6) and their temperature dependence had to be included in the iterative procedure.

The gas temperature used in the calculation should be the adiabatic wall temperature. This is nearly the same as the stagnation temperature, particularly in the throat region. The temperature used in the calculation was the stagnation temperature calculated from thermodynamic considerations.

The thickness of the alumina layer enters into Equations (21) and (23). Alumina-layer thicknesses were obtained from the chamber-pressure variation in the rocket motor. Because of the small size of the nozzle throat, the chamber pressure was particularly sensitive to the deposit-layer thickness at the throat. Variation in propellant burning rate with pressure was accounted for in the calculation. The deposit thickness computed for the end of the firing compared well for each test with the postfiring measurement. Although deposit thickness could be measured throughout the nozzle, the data were insufficient to provide an alumina-layer thickness history except at the throat. Therefore, the detailed heat-transfer-coefficient analyses were carried out only at the throat. Pressure dependence on alumina layer thickness is discussed further in the Appendix.

TEST-FIRING RESULTS

Five molybdenum calorimeter nozzles were fired for approximately 10 seconds each. Two of these firings were with Propellant A and three were with Propellant B. A new nozzle was used in each test firing.

Figures 4 and 5 show measured temperatures typical of those obtained with Propellants A and B, respectively. The thermocouple numbers used in Figures 4 and 5 correspond to those in Figure 2. The highest temperatures were generally attained in the region where the cone faired into the cylinder, i. e., Station 3. The temperatures tended to be only slightly lower at Stations 2 and 4. Axial conduction within the nozzle was important and could not be neglected in the \dot{q}_n calculation. Heat losses at the end of the nozzle were considered to be small even when compared with the axial heat transfer within the nozzle.

The measured temperatures increased rapidly during the tests. In each of the Propellant B motor tests, the measured temperatures exceeded the 4000 F calibrated limit of the tungsten-rhenium thermocouples at several locations. Postfiring examinations of the nozzles tested with Propellant B indicated that some surface melting of molybdenum had occurred. The location of the melting corresponded to the locations where the thermocouples had exceeded their calibration limit.

There is a tendency for the surface temperature to rise rapidly early in a firing, fall, and then rise again. The second rise continues throughout the remainder of the firing. This tendency was particularly pronounced in the case of Propellant A. The temperature fall is probably associated with the initial alumina deposit, which partially insulates the surface layer while it is being cooled through heat absorption by the bulk of the nozzle which is still cool.

Figure 6 shows a chamber pressure-time curve for the motor with Propellant A. The chamber pressure shows a minimum value following ignition, which approximately corresponds in time to the temperature peak. Also, the chamber pressure is a maximum at approximately the same time that the temperature begins its final climb.

Superimposed on the over-all trends are relatively high-frequency temperature oscillations. These are probably the result of build-up and slough-off of alumina from the surface. Similar oscillations appear to exist in the measured pressure, which tends to confirm this explanation.

The measured temperatures were used to compute heat-transfer coefficients at the nozzle throat by the method described previously. The high-frequency temperature oscillations were removed from the temperature curves prior to the calculation. The calculation was carried out for a time period which followed the alumina-layer establishment and during which the alumina-layer thickness was approximately constant. This corresponds to the times during which the alumina-layer heat-transfer analysis described previously is valid.

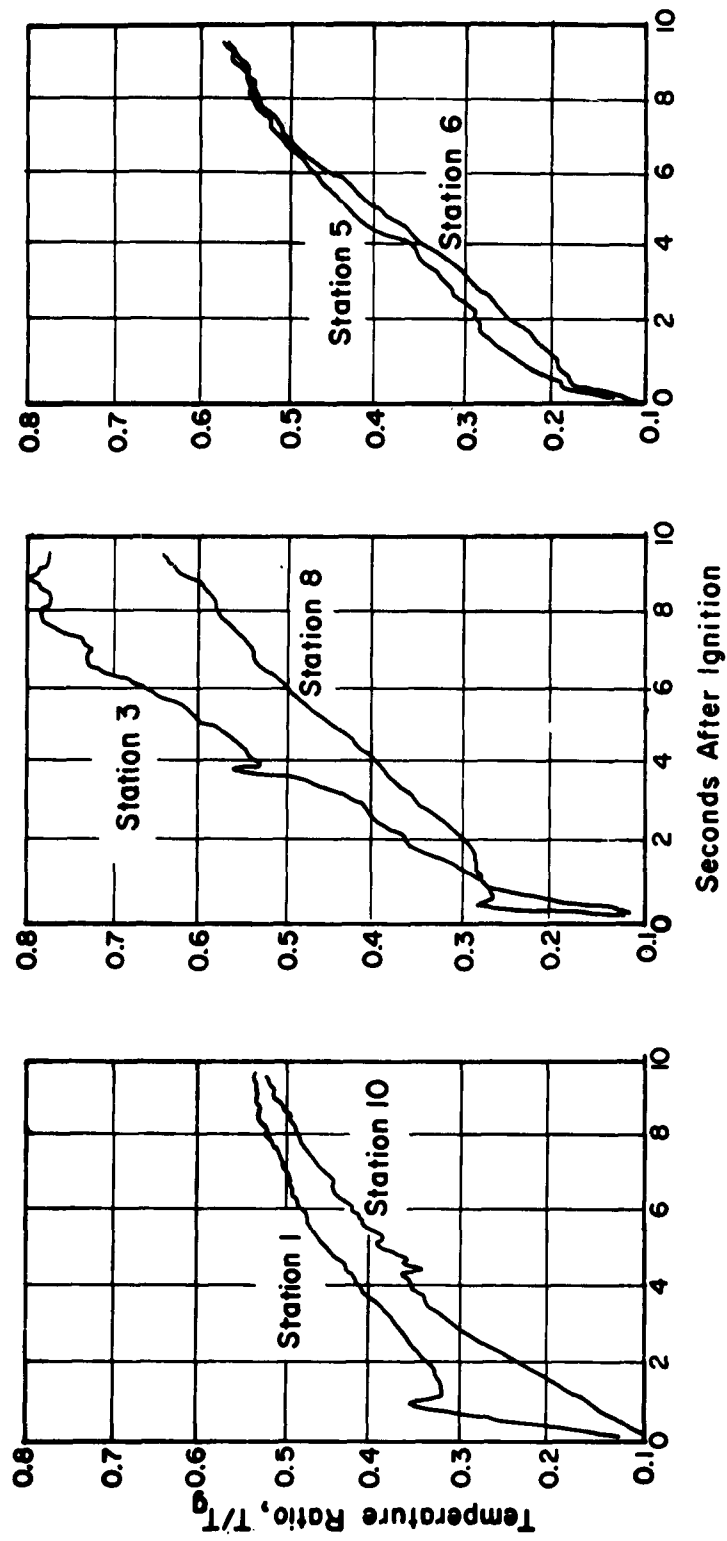


FIGURE 4. TYPICAL TEMPERATURE HISTORIES FOR PROPELLANT A

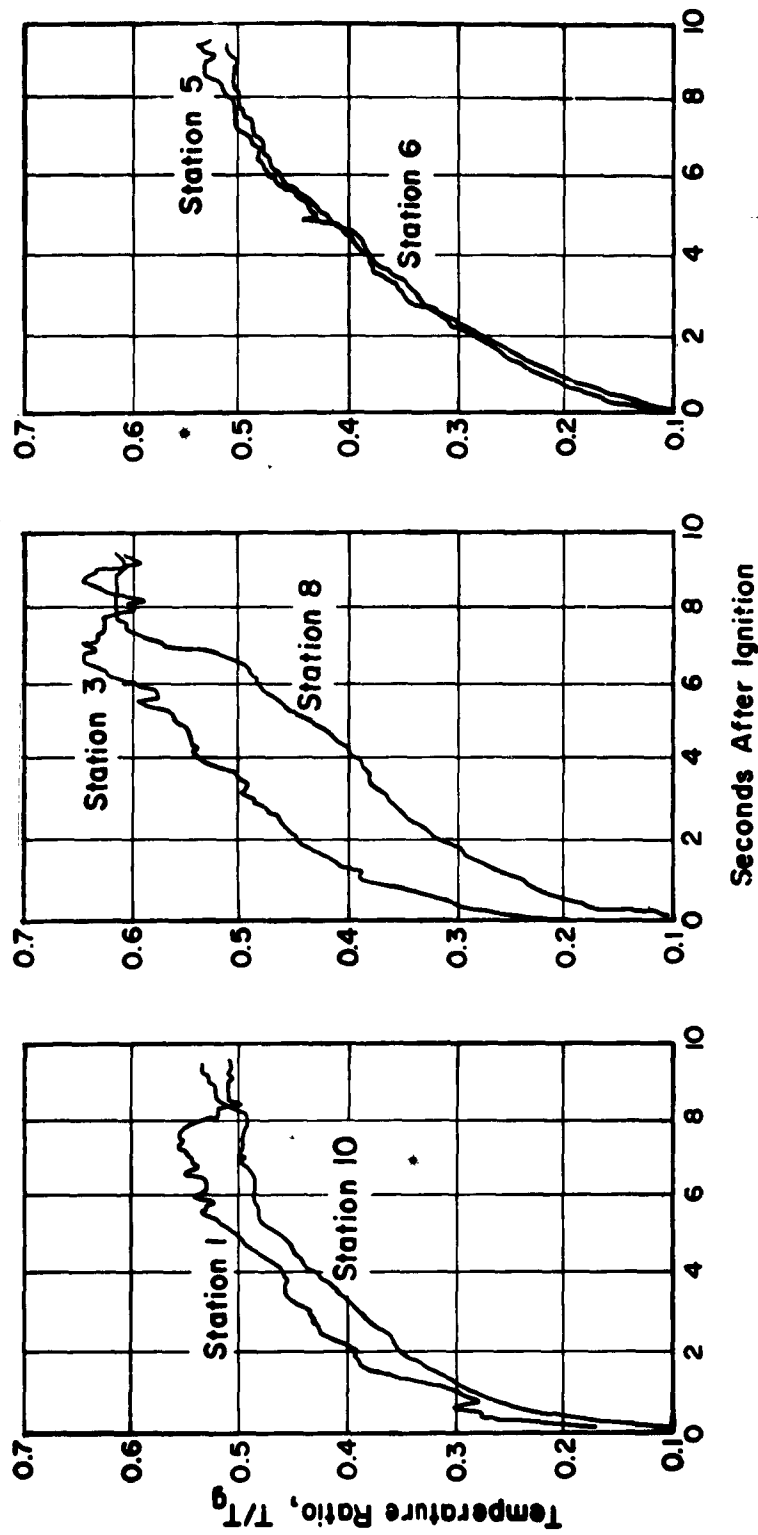


FIGURE 5. TYPICAL TEMPERATURE HISTORIES FOR PROPELLANT B

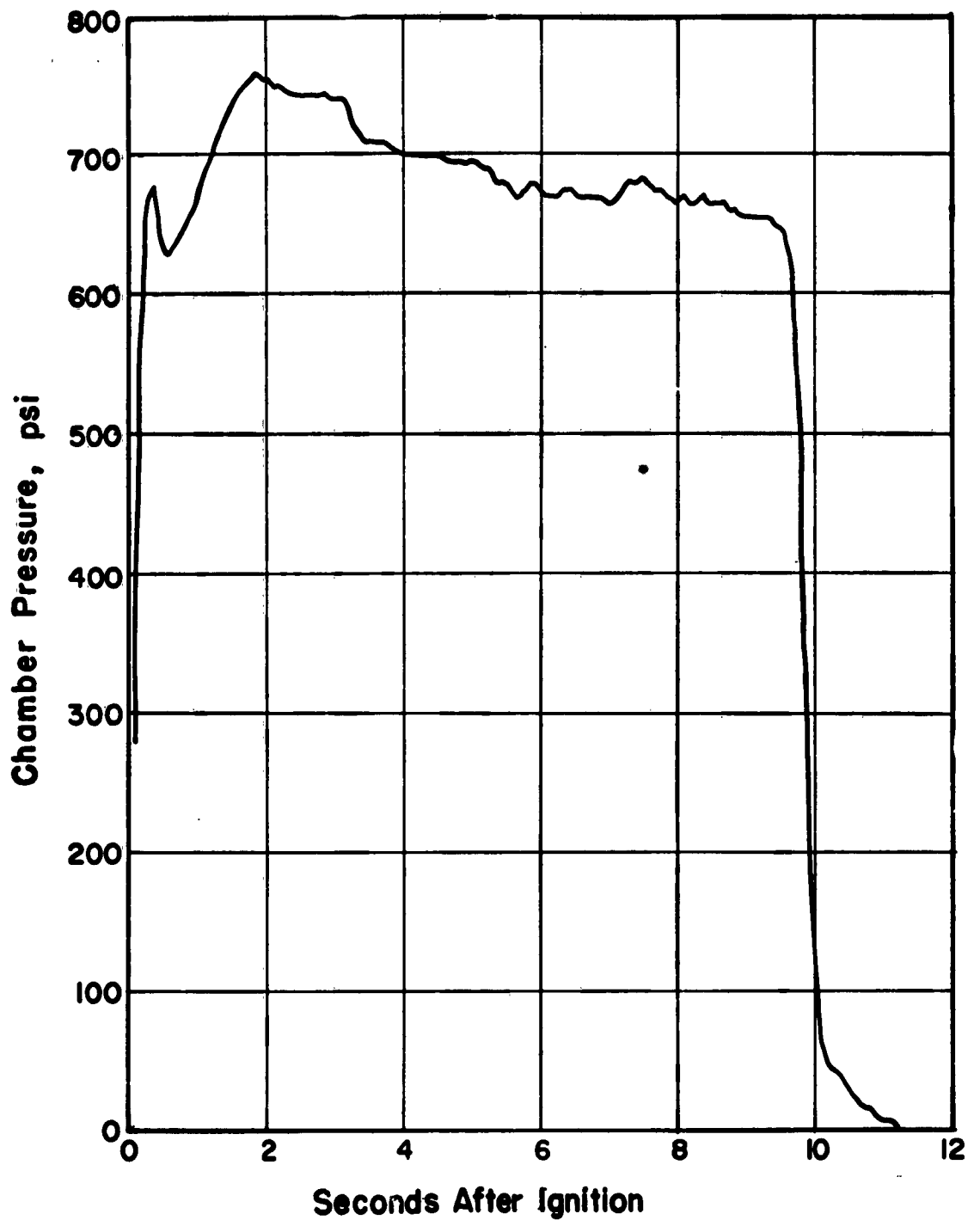


FIGURE 6. CHAMBER-PRESSURE TRACE FOR PROPELLANT A MOTOR

Table 1 shows the mean value of the computed heat-transfer coefficients for Propellants A and B. These heat-transfer coefficients are compared with calculated values based on the method of Bartz⁽⁷⁾. Bartz's approximate calculation procedure is based on the similarity between nozzle and turbulent pipe flows. In applying the Bartz method, no account was taken of the heat transferred to the alumina layer by aluminum oxide particles. The correspondence between the experimental and theoretical values of the heat-transfer coefficient is an indication that the particles have no significant effect on the heat-transfer process. Thus the heat-transfer coefficient should be correlated by

$$Nu = 0.026 Re^{0.8} Pr^{0.4}. \quad (25)$$

TABLE 1. HEAT-TRANSFER COEFFICIENTS

Propellant	Computed From Experiment, Btu/in. ² sec °F	Computed From Reference ⁽⁷⁾ , Btu/in. ² sec °F
A	$4.68 \times 10^{-3} \pm 8\%$ at 700 psig	4.05×10^{-3} at 700 psig
B	$3.18 \times 10^{-3} \pm 1.3\%$ at 675 psig	3.42×10^{-3} at 675 psig

Colucci⁽⁸⁾ suggested a correlation similar to Equation (25). However, the data presented by Colucci for an aluminized propellant could not be correlated by Equation (25) except in a region of the nozzle exit cone where there were no deposits.

The heat-transfer coefficient calculation was, of course, dependent on the calculation of the temperature at the exposed alumina surface, T_A . The temperature difference across the alumina layer was found to be of the order of 1000 to 2000 F. There was a time period during the firing when the temperature T_A was essentially constant and approximately equal to the melting point of alumina. This should be expected for a portion of the time when the alumina thickness is decreasing. Eventually, the alumina surface temperature approaches the alumina melting point and the temperature T_A begins to rise again. This occurred earlier in the firings with Propellant B than with A because of its higher flame temperature.

TEMPERATURE-HISTORY CALCULATIONS

The heat-transfer coefficients obtained from the experiments described in the previous section were applied to the calculation of the temperature history of some ceramic materials which had been previously tested as nozzle inserts* with the propellants used in the present study. Since ceramics generally have low thermal conductivities, it is reasonable to apply a solution to the heat-conduction equation which neglects axial conduction.

The throat region of the nozzle is a cylinder. Mayer⁽⁹⁾ showed that the temperature in a thick-walled cylinder heated on the inside and insulated on the outside is

$$\theta = \frac{T}{T_g} = 1 + \sum_{n=1}^{\infty} A_n R_o(\mu_n \omega) e^{-\mu_n^2 \tau_a} , \quad (26)$$

where

$$A_n = \frac{-2N_a R_o(\mu_n)}{(\mu_n \Omega)^2 R_o^2(\mu_n \Omega) - (\mu_n^2 + N_a^2) R_o^2(\mu_n)} ,$$

$$\Omega = \frac{b}{a} ,$$

$$\omega = \frac{r}{a} ,$$

$$\tau_a = \frac{at}{a^2} ,$$

$$N_a = \frac{U_o d}{k} ,$$

$$R_o(\mu_n) = \frac{J_o(\mu_n)}{J_1(\mu_n \Omega)} - \frac{Y_o(\mu_n)}{Y_1(\mu_n \Omega)} ,$$

* Design was the same as that shown in Figure 2.

and a is the cylinder inside radius, b is the outside radius, d is the thickness, the J 's are Bessel functions of the first kind, and the Y 's are Bessel functions of the second kind. U_o is an over-all heat-transfer coefficient which includes both the gas-side heat-transfer coefficient h and the thermal resistance of the alumina layer. It is defined in the usual manner by

$$U_o = \frac{1}{\frac{1}{h} + \frac{r_o}{k_A} \ln \left(\frac{r_o}{r_o - \delta} \right)},$$

where k_A is the thermal conductivity of the alumina.

The eigenvalue μ is determined by solving the equation

$$-\mu_n \frac{R_1(\mu_n)}{R_o(\mu_n)} = N_a, \quad (27)$$

where

$$R_1(\mu_n) = \frac{J_1(\mu_n)}{J_1(\mu_n \Omega)} - \frac{Y_1(\mu_n)}{Y_1(\mu_n \Omega)}.$$

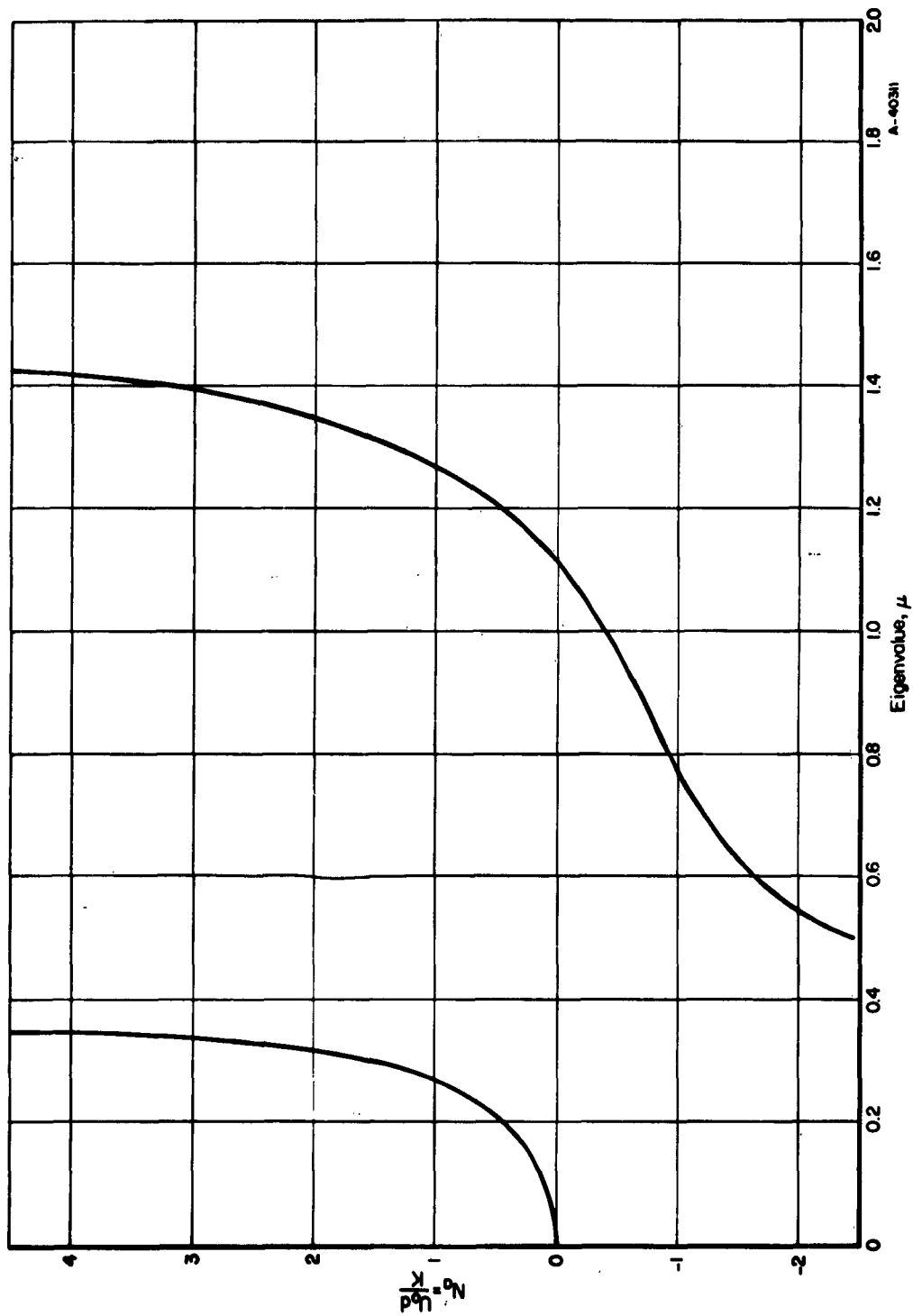
At the inside surface, $\omega = 1$, so that Equation (26) can be expressed as

$$\theta_s = 1 - \frac{2}{N_a} \sum_{n=1}^{\infty} \frac{e^{-\mu_n^2 \tau_a}}{\left[\frac{\Omega^2 R_o^2(\mu_n \Omega) - R_o^2(\mu_n)}{R_1^2(\mu_n)} - 1 \right]}. \quad (28)$$

Figure 7 is a plot of Equation (27) for $\Omega = 4$ which corresponds to the nozzle used in this study. It shows that, for values of $N_a > 2.5$, μ is essentially independent of N_a . In the rocket nozzle under consideration, N_a is of the order 4.

The order of magnitude difference between μ_1 and μ_2 should also be noted. A sample calculation showed that the μ_2 term in the expansion of Equation (28) was negligible compared to the μ_1 term. Thus, only the first term in the series of Equation (28) is required for τ_a appreciably greater than zero. Additional terms are needed for early times.

This analysis cannot be applied to the prediction of the nozzle surface-temperature history prior to firing because the alumina-layer thickness at each point in time must be obtained from the motor chamber pressure by the

FIGURE 7. EIGENVALUE VARIATION WITH N_a

method described in the Appendix. Further, the heat-transfer coefficient depends on chamber pressure. On the basis of Equation (25), the heat-transfer coefficients of Table 1 should be corrected by an 0.8 power for variation in chamber pressure. In applying the results, however, a linear chamber-pressure correction was used to account additionally for changes in the burning conditions.

The best available thermal-property data were applied to the calculation. There is considerable uncertainty in the high-temperature values of these properties for ceramics.

Equation (28) is a solution to the heat-conduction equation for constant thermal properties. Over the temperature range of interest, thermal properties vary considerably. In order to minimize errors from this source, the values of the thermal properties were averaged over the temperature range encountered in the rocket-motor firing. The mean values used in the calculations are shown in Table 2.

TABLE 2. MEAN PROPERTY VALUES FOR VARIOUS CERAMICS

Material	Density, lb/in. ³	Thermal Conductivity, 10 ⁻⁴ Btu/sec-in. -°F	Specific Heat, Btu/lb -°F
Niobium carbide	0.253	3.86	0.123
Tantalum carbide	0.455	4.74	0.069
GRB silicon carbide	0.101	7.44	0.374
ZT graphite	0.074	7.80	0.430

The over-all heat-transfer coefficient was averaged at each point in time from motor ignition. Thus, at each point in time

$$U_{o,N} = \frac{1}{N} \sum_{i=1}^N U_{o,i} \quad , \quad (29)$$

where $U_{o,i}$ is the thermal conductivity at each time increment and N is the total number of time increments.

Time increments of 0.5 second were used in the calculation. An average, taken in the manner of Equation (29), is considered to be properly weighted to account for the variation in the heat-transfer coefficient and alumina-layer thickness during firing. The validity of this approach improves with time. It is not considered valid during the period of initial alumina-layer build-up.

Mayer⁽⁹⁾ presented numerical results based on a value of $\Omega = 2$ and $N_a = 1$. Comparison with calculations of θ_s for the nozzles of interest showed that correction of the Mayer results by the actual value of N_a in the manner indicated by Equation (28) yielded sufficiently accurate values of θ_s .

Figures 8 and 9 show calculated surface temperatures at the nozzle throat for Propellant A and Propellant B, respectively. Also shown in the figures are several measured temperature histories with their fluctuations (see Figures 4 and 5) removed. Agreement between measured and calculated temperatures is considered to be good when thermal-property differences (in the case of molybdenum) and thermocouple depth are accounted for. Not too much faith should be placed in the calculated temperatures during the first 2 seconds of motor firing, i. e., during the alumina-layer build-up period. However, beyond 2 seconds, the temperatures appear to be quite reasonable. The calculated temperatures successfully predicted the time in the firing at which several of the ceramic materials failed by melting or thermal degradation.

CONCLUSIONS

The effects of the aluminum oxide deposit layer must be included in the analysis of nozzle heat transfer. Because alumina has a relatively low thermal conductivity and the deposit layer is thin, it is possible to approximate the heat-transfer equations by the steady-state relations with a small correction applied to heat flux.

Once the presence of the alumina layer is properly accounted for, it appears that a standard turbulent heat-transfer correlation is reasonably correct at the throat. Detailed analyses were not carried out in the converging section of the nozzle because the deposit-layer thickness was not known as a function of time. The thickness of the layer depends on the deposit rate from the gas stream and also on the flow conditions on the nozzle surface. The alumina-layer flow problem is considered particularly difficult because the properties (and phase) are strongly dependent on temperature.

The results of this study were used to successfully predict the throat surface temperature of several ceramic materials. Calculations based on available thermal-property data successfully predicted the time in the firing at which melting or thermal degradation occurred. For these calculations, alumina deposit-layer thicknesses had to be inferred from measured pressure histories. Completely a priori prediction of the temperature history must await an improved alumina-layer theory.

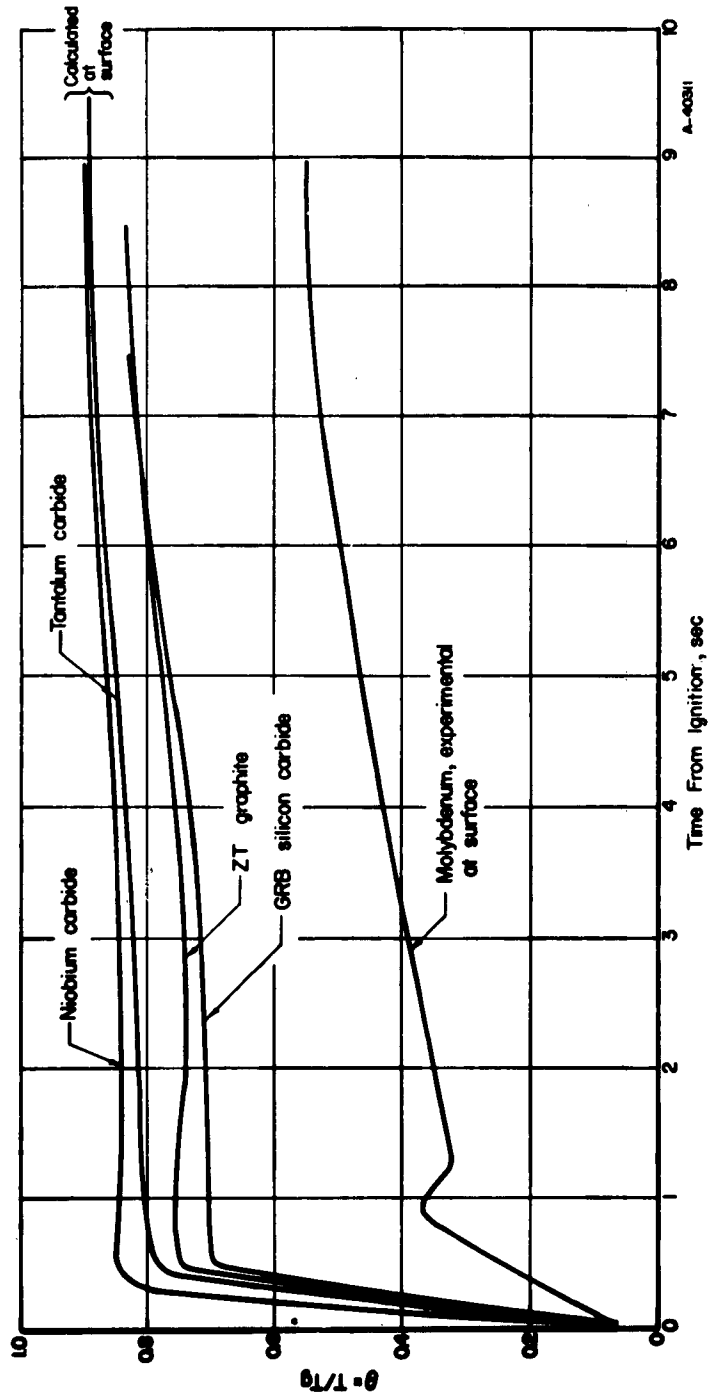


FIGURE 8. CALCULATED AND EXPERIMENTAL SURFACE TEMPERATURES OF NOZZLE INSERTS FIRED IN MOTORS CONTAINING PROPELLANT A

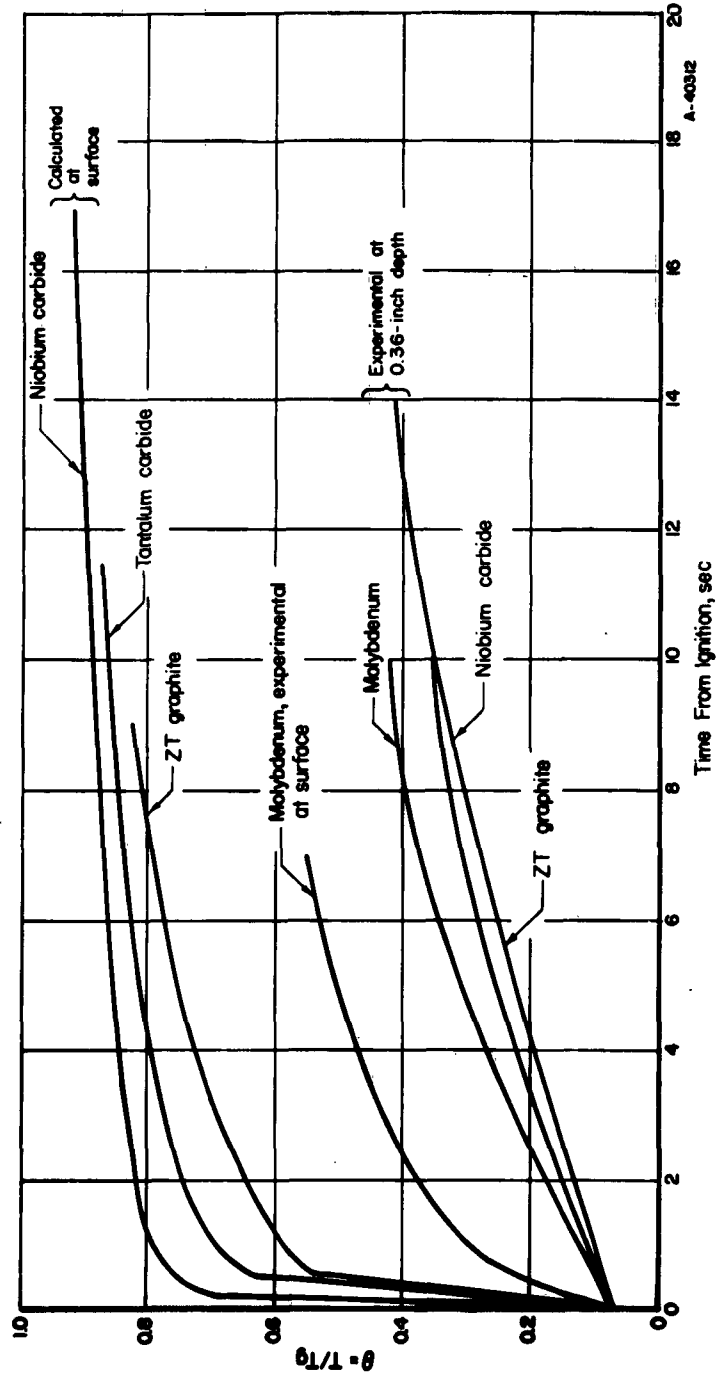


FIGURE 9. CALCULATED AND EXPERIMENTAL SURFACE TEMPERATURES OF NOZZLE INSERTS FIRED IN MOTORS CONTAINING PROPELLANT B

REFERENCES

- (1) Jakob, M. , Heat Transfer, Vol. 1, John Wiley & Sons, Inc. , New York (1949), p 377.
- (2) Dusinberre, G. M. , Numerical Analysis of Heat Flow, McGraw-Hill Book Company, New York (1949), p 114.
- (3) Rasor, N. S. , and McClelland, J. D. , "Thermal Properties of Materials, Part 1", WADC TR 56-400, ASTIA Doc. No. AD 118144 (March, 1957).
- (4) Goldsmith, A. , and Waterman, T. E. , "Thermophysical Properties of Materials", WADC TR 58-476, ASTIA Doc. No. AD 207905 (January, 1959).
- (5) Carslaw, H. S. , and Jaeger, J. C. , Conduction of Heat in Solids, 2nd Edition, Oxford Press, London (1959), pp 103, 31.
- (6) McQuarrie, M. , "Thermal Conductivity: VII, Analysis of Variation of Conductivity With Temperature for Al_2O_3 , BeO, and MgO", Journal of the American Ceramic Society, 37 (2), Part 2, 91 (February, 1954).
- (7) Bartz, D. R. , "A Simple Equation for Rapid Estimation of Rocket Nozzle Convective Heat Transfer Coefficients", Jet Propulsion, 27 (1), 49 (January, 1957).
- (8) Colucci, S. E. , Experimental Determination of Solid Rocket Nozzle Heat Transfer Coefficient, Proceedings of the Fifth Symposium on Ballistic Missile and Space Technology, Vol. II, Academic Press, New York (1960), p 303.
- (9) Mayer, E. , "Analysis of Temperature Transients in Rocket Walls", M. W. Kellog Report, SPD 169 (1948).

EU/mln

APPENDIX

PRESSURE DEPENDENCE ON ALUMINA THICKNESS

BATTELLE MEMORIAL INSTITUTE

APPENDIX

PRESSURE DEPENDENCE ON ALUMINA THICKNESS

The mass flow of combustion products through a rocket motor can be approximated by

$$\dot{m} = \rho A_n u \quad , \quad (A-1)$$

or in terms of total pressure and temperature

$$\dot{m} = C_1 \sqrt{\frac{\gamma}{RT_0}} \frac{P_0 A_n M}{\left(1 + \frac{\gamma-1}{2} M^2\right)^{\frac{\gamma+1}{2(\gamma-1)}}} \quad , \quad (A-2)$$

where C_1 is a constant which is introduced to account for the flow coefficient and for deviations from a perfect gas.

In addition, for solid propellants, the burning rate is proportional to the chamber pressure raised to the exponent n (where for most propellants $n < 1$). The value of the pressure exponent is generally a known property of the propellant. Thus, for a constant burning area, which is usually well approximated by end-burning propellant grains,

$$\dot{m} = C_2 P_0^n \quad . \quad (A-3)$$

In order to evaluate the thickness of the alumina layer on the basis of the measured chamber pressure, Equations (A-2) and (A-3) are combined to eliminate the mass flow rate. Thus,

$$P_0^{n-1} = \frac{C_1}{C_2} \sqrt{\frac{\gamma}{RT_0}} \frac{\pi r^2 M}{\left(1 + \frac{\gamma-1}{2} M^2\right)^{\frac{\gamma+1}{2(\gamma-1)}}} \quad . \quad (A-4)$$

It is noted that at the throat $M = 1$. Also because of the uncertainties in the knowledge of T_0 , γ , and R , it is convenient to consider terms containing these quantities as part of the constant. Thus, Equation (A-4) can be rewritten as

$$r = \frac{P_0^{\frac{n-1}{2}}}{C_3} \quad . \quad (A-5)$$

It is further noted that

$$\delta = r_o - r \quad , \quad (A-6)$$

where r_o is the nozzle throat radius prior to firing. Thus,

$$\delta = r_o - \frac{P_o^{\frac{n-1}{2}}}{C_3} \quad . \quad (A-7)$$

The constant C_3 was determined on the basis of the motor-design conditions. This condition was found to be valid for firings with pyrolytic graphite nozzles. These nozzles had a sufficiently high surface temperature to be free of alumina deposits during firing.

Figure A-1 shows plots of Equation (A-7) for two nozzles which were fired with Propellant A and Propellant B, respectively. The value of r_o was determined by measurement prior to firing. It should be noted that the sensitivity of measured chamber pressure to alumina layer thickness is approximately 9×10^{-5} in./psi.

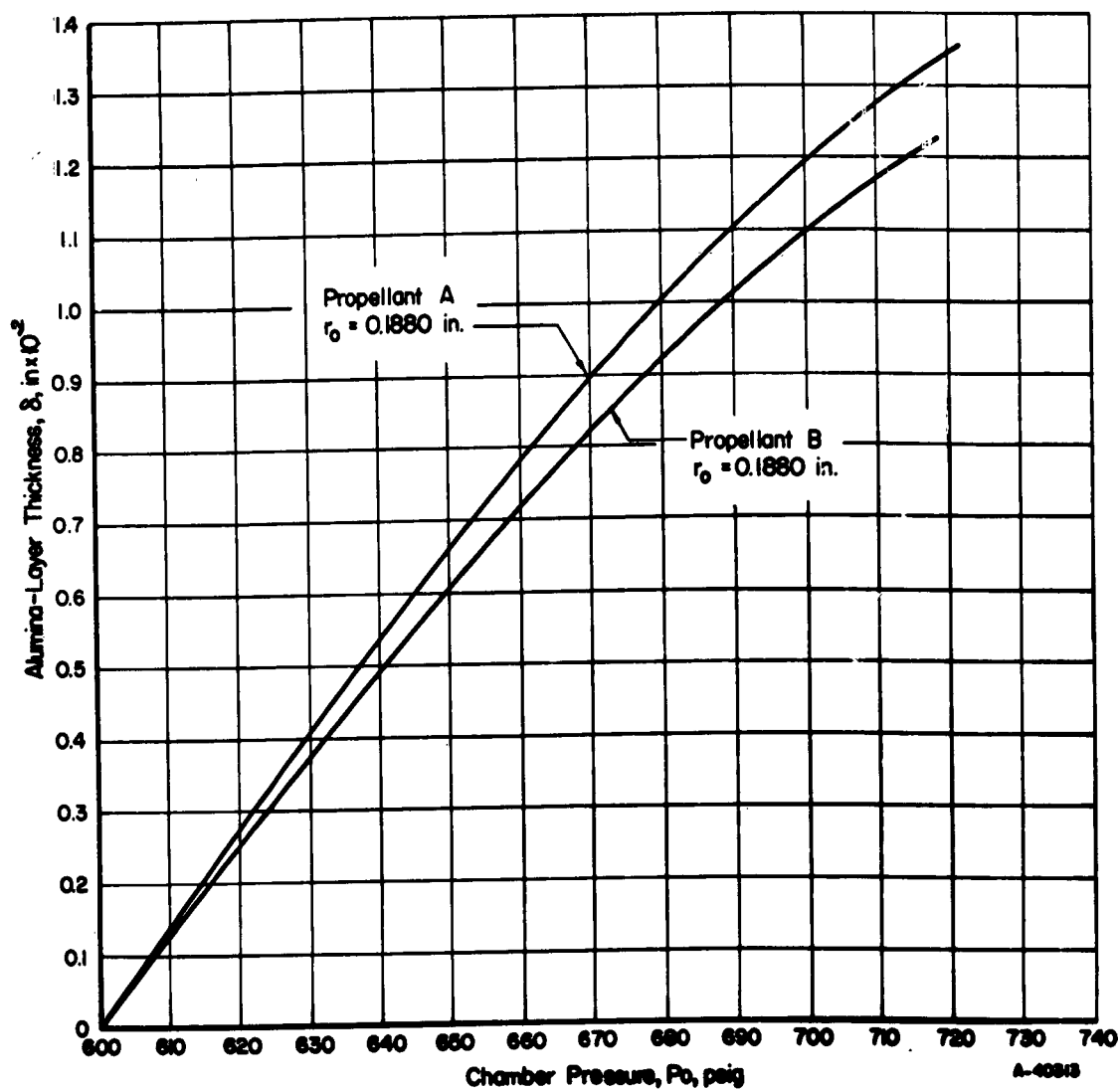


FIGURE A-1. VARIATION OF ALUMINA-LAYER THICKNESS AS A FUNCTION OF MEASURED CHAMBER PRESSURE